6440 *Biochemistry* **2010,** *49,* 6440–6450
DOI: 10.1021/bi1005915

BIOCHEMISTRY
including biophysical chemistry & molecular biology
Article

Crystal Structure of the Nosiheptide-Resistance Methyltransferase of *Streptomyces actuosus*[†,‡]

Huirong Yang,[¶,§,∥,⊥] Zhe Wang,[¶,∥,#] Yan Shen,[¶,∥,#] Ping Wang,[¶,∥,⊥] Xu Jia,[∥,#] Liang Zhao,[∥,△] Pei Zhou,[#] Rui Gong,[∥,⊥] Ze Li,[∥,⊥] Ying Yang,[∥,⊥] Dongrong Chen,*[,∥,#] Alastair I. H. Murchie,*[,∥,#] and Yanhui Xu*[,§,∥,⊥]

[§]*Cancer Institute, Shanghai Cancer Center, Fudan University, and Department of Oncology, Shanghai Medical College, Fudan University, Shanghai 200032, China,* [∥]*Institutes of Biomedical Sciences, Fudan University, 130 Dong-An Road, Shanghai 200032, China,* [⊥]*School of Life Sciences, Fudan University, 220 Han-Dan Road, Shanghai 200433, China,* [#]*Department of Pharmacy, Fudan University, Shanghai 201203, China, and* [△]*Department of Chemistry, Fudan University, Han-Dan Road, Shanghai 200433, China* [¶]*These authors contributed equally to this work*

Received April 19, 2010; Revised Manuscript Received June 10, 2010

ABSTRACT: Nosiheptide-resistance methyltransferase (NHR) of *Streptomyces actuosus* is a class IV methyltransferase of the SpoU family and methylates 23S rRNA at nucleotide adenosine corresponding to A1067 in *Escherichia coli*. Such methylation is essential for resistance against nosiheptide, a sulfur peptide antibiotic, which is produced by the nosiheptide-producing strain, *S. actuosus*. Here, we report the crystal structures of NHR and NHR in complex with SAM (*S*-adenosyl-L-methionine) at 2.0 and 2.1 Å resolution, respectively. NHR forms a functional homodimer, and dimerization is required for methyltransferase activity. The monomeric NHR is comprised of the N-terminal RNA binding domain (NTD) and the C-terminal catalytic domain (CTD). Overall, the structure of NHR suggests that the methyltransferase activity is achieved by "reading" the RNA substrate with NTD and "adding" methyl group using CTD. Comprehensive mutagenesis and methyltransferase activity assays reveal critical regions for SAM binding in CTD and loops (L1 and L3) essential for RNA recognition in NTD. Finally, the catalytic mechanism and structural model that NHR recognizes 23S rRNA is proposed based on the structural and biochemical analyses. Thus, our systematic structural studies reveal the substrate recognition and modification by the nosiheptide-resistance methyltransferase.

The development of resistance to antibiotics is an increasing clinical problem. It is therefore important to understand the mechanism of antibiotic resistance. Several classes of antibiotics target the bacterial ribosome and specifically inhibit bacterial protein synthesis. The crystal structures of 30S, 50S, and 70S ribosomes (*1*−*4*) have improved our understanding of the mode of action for many ribosome-binding antibiotics, including the aminoglycosides, tetracyclines, and macrolides (*5*, *6*). These antibiotics interact with key functional sites within the ribosome and interfere with essential steps in protein synthesis such as peptide bond formation, GTP hydrolysis, and mRNA decoding. Resistance to antibiotics that target the bacterial ribosome is often conferred by methylation at specific rRNA nucleotides, which are usually located at the site of antibiotic interaction. *S*-Adenosyl-L-methionine (SAM[1] or AdoMet) dependent methyltransferases are responsible for the specific methylation process. For example, Erm is responsible for macrolide−lincosamide−streptogramin resistance (*7*−*9*). 16S rRNA methyltransferase FmrO from *Microspora olivasterospora* is involved in fortimicin A resistance (*10*). AviRb from *Streptomyces viridochromogenes* mediates resistance to the oligosaccharide antibiotic avilamycin (*11*), and RlmB from *Escherichia coli* is predicted to inhibit certain antibiotics (*12*). TSR (thiostrepton-resistance methyltransferase) from *Streptomyces azureus* is responsible for the resistance to thiostrepton (*13*−*16*), and NHR (nosiheptide-resistance methyltransferase) from *Streptomyces actuosus* mediates resistance to nosiheptide (*17*, *18*).

Nosiheptide is a sulfur peptide antibiotic and belongs to a family of thiazole antibiotics (*19*, *20*). It has been used in veterinary medicine for its capability against Gram positive bacteria (*21*). Nosiheptide binds to the 50S subunit of the ribosome and inhibits hydrolysis of GTP by elongation factor G (EF-G), inhibiting ribosomal translocation and elongation (*16*, *22*, *23*). The mechanism employed by the nosiheptide producer *S. actuosus* for self-protection from the antibiotic is through the 2′-O-methylation of position A1067 in helix 43 (H43) of 23S rRNA (*14*, *16*−*18*, *24*) . Structural analysis of ribosomes with nosiheptide bound shows that it binds close to the 2′-O position of A1067; thus methylation of A1067 blocks thiazole binding directly (*13*, *25*, *26*). Through methylation at A1067 of 23S rRNA by NHR, the ribosome of *S. actuosus* becomes

[†]This work was supported by Project 985 from the Ministry of Education, China (P.R.), and by grants from the National Natural Science Foundation of China (30870493), National Basic Research Program of China (2009CB918600), Shanghai Pujiang Program (08PJ14010), Ministry of Science and Technology of China (2009ZX09503-006), Shanghai National Natural Science Foundation (10ZR1402800 and 30970061), Shanghai Leading Academic Discipline Project (B111), and Graduate Student Innovation Foundation of Fudan University.

[‡]Coordinates and structure factors for the NHR and NHR complex with SAM crystal structures have been deposited in the RCSB PDB with accession numbers 3NK6 and 3NK7, respectively.

*To whom correspondence should be addressed. D.C.: tel, 86-21-54237577; fax, 86-21-54237577; e-mail, drchen@fudan.edu.cn. A.M.: tel, 86-21-54237577; fax, 86-21-54237577; e-mail, aihm@fudan.edu.cn. Y.X.: tel, 86-21-54237294; fax, 86-21-54237294; e-mail, xuyh@fudan.edu.cn.

[1]Abbreviations: NHR, nosiheptide-resistance methyltransferase; SAM, *S*-adenosyl-L-methionine; NTD, N-terminal RNA binding domain; CTD, C-terminal catalytic domain; SAD, single-wavelength anomalous dispersion; MTase, methyltransferases.

 Published on Web 06/15/2010

self-protected. The specific methylation at A1067 in 23S rRNA occurs between nucleotides 1051−1108 in a region of rRNA that can fold independently, is the binding site for the ribosomal protein L11 (*27*−*30*), and is an efficient substrate for the (TSR) thiazole resistance methyltransferases (*13*, *31*, *32*).

Based on the amino acid sequence alignments, NHR is predicted to belong to the SpoU family of tRNA and rRNA ribose 2′-*O*-methyltransferases that share a series of common sequence motifs (*33*, *34*). The SpoU family of methyltransferases also shares a series of common sequence motifs with the TrmD family of tRNA methyltransferases (*35*, *36*). The crystal structures of TrmH and several TrmD proteins (*33*, *35*, *37*) reveal them to have a similar tertiary fold, suggesting that they share a common evolutionary origin. The SpoU family has therefore been combined with the TrmD methyltransferases to make up a "SPOUT" (SpoU-TrmD) superfamily. Several structures of the RNA methyltransferases described above have been reported. However, the structure of NHR and the molecular mechanism of NHR-mediated 23S rRNA recognition and methylation remain unknown.

Here, we report the crystal structures of NHR (at 2.0 Å resolution) and NHR complexed with SAM (at 2.1 Å resolution). Comprehensive structural and biochemical analyses revealed critical regions for SAM binding in CTD and loops (L1 and L3) essential for RNA recognition in NTD. These systematic studies allow us to propose a molecular mechanism of substrate 23S rRNA recognition and modification mediated by nosiheptide-resistance methyltransferase.

MATERIALS AND METHODS

Protein Expression, Purification, and Crystallization. The CDS of *Nhr* and *Tsr* were amplified by PCR using genomic DNA from *S. actuosus* and *S. azureus* as templates and then inserted into pET28a and pETduet vectors (Novagen). All constructs were generated using a PCR-based cloning strategy, and all mutants were generated by the QuickChange mutagenesis protocol (Stratagene). Protein expression, purification, and crystallization of NHR have been reported (*38*). Briefly, His-tagged TSR, NHR, and NHR mutants were expressed at 15 °C in *E. coli* strain BL21(DE3). Cells were harvested and resuspended in buffer A containing 25 mM Tris-HCl (pH 8.0), 150 mM NaCl, and 5 mM imidazole, supplemented with DNase and protease inhibitors. The soluble fraction of cell lysate was loaded onto a Ni-NTA (GE Healthcare) affinity column. The protein was eluted and further purified by ion-exchange chromatography (Source 15Q; GE Healthcare) followed by gel filtration (Superdex 200; GE Healthcare) and concentrated to 10 mg/mL for crystallization. The crystals of NHR were grown by the hanging-drop vapor diffusion method at 18 °C by mixing 1 μL of protein solution and 1 μL of reservoir solution containing 0.35 M NH_4Cl, 24% PEG3350, and 100 mM MES (pH5.7). Because NHR shared only 23% identity with the best hit (1IPA.pdb) in a PDB search using the primary sequence, we also prepared selenomethionine derivative crystals for data collection just in case the structure could not be solved by molecular replacement. The selenomethionine derivative of NHR was expressed in M9 medium containing 60 mg L^{-1} selenomethionine in BL21(DE3). The derivative crystals were obtained using similar conditions to those of native crystals.

Data Collection and Structure Determination. All crystals were flash-frozen in liquid nitrogen with reservoir solution as cryoprotectant. Data collection was carried out at beamline BL17A of the Photon Factory (Japan) and beamline BL17U at SSRF (Shanghai Synchrotron Radiation Facility in China). The program HKL2000 was used for data processing (*39*). Phases for NHR were initially determined by the single-wavelength anomalous dispersion (SAD), and automatic model building was performed by using the program package PHENIX (*40*). More than 40% of residues in one asymmetric unit were traced into the experimental electron density map. The remaining residues were manually built with COOT (*41*). The complex model with SAM was accomplished using the native structure (2.0 Å). All refinements were performed with the program package PHENIX (*40*). The final models were evaluated by PROCHECK, which showed a good stereochemistry according to the Ramachandran plot (*42*). The structure similarity search was performed with the DALI Server (*43*).

RNA Preparation and Purification. The DNA templates containing the T7 RNA polymerase promoter sequence for transcription were obtained by gene synthesis. RNA was transcribed *in vitro* by T7 RNA polymerase. RNA was purified by gel electrophoresis in a 10% polyacrylamide 7M urea gel, and RNA was collected by electroelution and recovered by ethanol precipitation. RNA concentrations were determined by a nanodrop spectrophotometer (ND-1000).

NHR/TSR in Vitro Methylation Assay. NHR and TSR methyltransferase activities were measured as described (*13*). Briefly, RNAs at the appropriate concentrations were incubated in the presence of either NHR or TSR methyltransferase in the presence of [^{14}C]SAM at 25 °C for 1 h. Reactions were stopped by the addition of 2% TFA, and the precipitate was filtered through a 96-well glass fiber filter plate. Incorporation of ^{14}C was determined by liquid scintillation counting in a MicroBeta TriLux (Perkin-Elmer 1450 LSC luminescence counter). K_M, the Michaelis constant, was calculated as previously described (*13*).

Mutant proteins were assayed at an RNA concentration close to the K_M for the RNA substrate (~350 nM for the 60 base RNA and ~200 nM for the 29 base RNA). The efficiency of mutant proteins was quantified as the proportion of ^{14}C incorporated into the substrate RNA as a percentage of the equivalent reaction by the wild-type protein.

RESULTS

In Vitro Reconstitution of Methyltransferase Activity of NHR and TSR. It has been reported that NHR is a methyltransferase for 23S rRNA at A1067 (*13*). To study the molecular mechanism of NHR-mediated rRNA methylation, we reconstituted the enzymatic reaction *in vitro* using purified NHR protein and both 60 nucleotide and 29 nucleotide 23S rRNA as substrates (Figure 1A,B). Both RNA molecules contain the substrate base for NHR positioned at A1067 within the H43 loop of ribosome. The *in vitro* methylation assay showed that NHR has methyltransferase activity for both substrates (Figure 1C,D). To confirm that the shortened 29 and 60 nucleotide RNA molecules were appropriate substrates for NHR, we synthesized a series of mutant 29-mer RNA molecules in which the A1067 position had been changed to G, C, or U; in each case methylation of the mutant RNA by NHR was greatly reduced compared to the corresponding natural rRNA sequence, such that A1067G (~5%) > A1067C (~2%) > A1067U (~1%). This suggests that the shorter RNA substrates mimic 23S rRNA sufficiently for

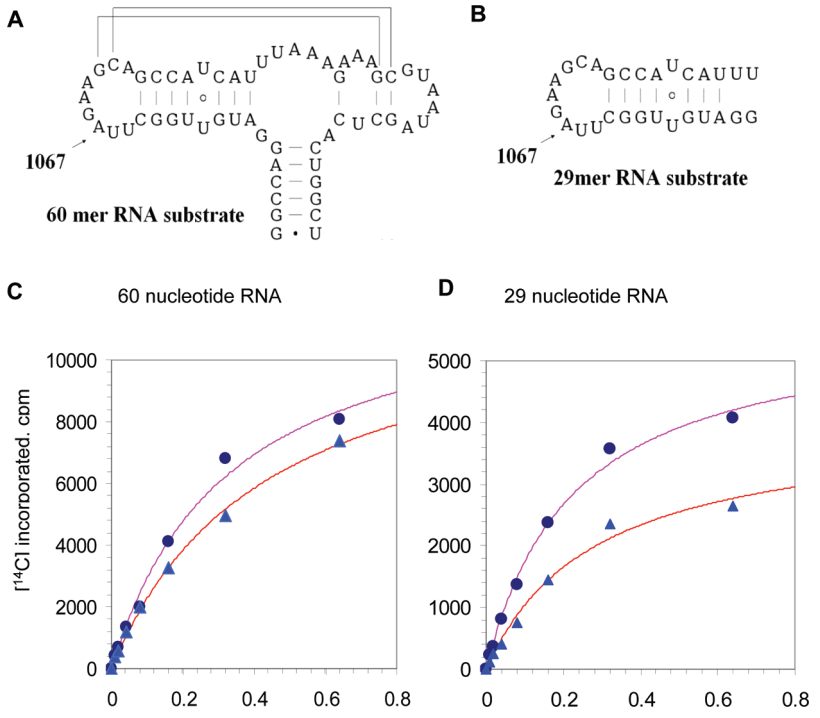

FIGURE 1: *In vitro* reconstitution of methyltransferase activity of NHR and TSR. (A) The secondary structure of the 60 base RNA substrate, corresponding to nucleotides 1051−1108 of 23S rRNA including H43 and H44 and the methyl group receptor base A1067. (B) The secondary structure of the 29 base RNA substrate corresponding to nucleotides 1055−1083 of 23S rRNA including only the H43 loop that includes the methyl group receptor base A1067. (C) Methyltransferase activity with the 60 base RNA as a substrate. A series of RNA dilutions corresponding to the concentrations shown in the figure were incubated with NHR (closed circles) or TSR (closed triangles) in the presence of [^{14}C]SAM at 25 °C for 1 h, RNA was precipitated with TFA, and methyl group incorporation was quantified by scintillation counting. Half-maximal incorporation was reached at 343 nM RNA for NHR and at 446 nM RNA for TSR. (D) Methyltransferase activity with the 29 base RNA as a substrate. RNA was incubated with NHR (closed circles) or TSR (closed triangles) in the presence of [^{14}C]SAM and precipitated. Half-maximal incorporation was reached at 221 nM RNA for NHR and at 284 nM RNA for TSR.

methylation of A1067, as has been previously noted for TSR (*14*). Intriguingly, the enzymatic activity (K_M) for the 60 nucleotide RNA is slightly lower than that for the 29 base RNA, indicating that 29 nucleotide RNA is a better substrate for this assay system. Since NHR and TSR share 74% sequence homology (Supporting Information Figure S1), we also compared the methyltransferase activity of the two proteins for both 60 nucleotide and 29 nucleotide RNA. TSR has slightly lower activity for both 29 and 60 nucleotide RNA than NHR (Figure 1C,D). The difference in enzymatic activity between NHR and TSR will be discussed below. The methyltransferase activity assays were used on wild type and mutants of NHR protein to verify the importance of specific residues according to the structural analysis.

Overall Structure of NHR. To investigate the substrate recognition and molecular mechanism of rRNA methylation, we solved the crystal structure of NHR and NHR in complex with SAM to 2.0 and 2.1 Å resolution, respectively (Figure 2A, Supporting Information Figure S2). Statistics of structure determination and refinement are summarized in Table 1.

Consistent with the results from gel filtration chromatography (*38*), the NHR crystal structure reveals one homodimer per asymmetric unit. For one monomer, residues 26−28 and 88−93 were not built because of weak electron density, while for the other residues 1−4 and 272−274 were not included. The two monomers were nearly identical with a root-mean-square deviation (rmsd) of 0.606 Å for 235 Cα atoms. Residues of 26−28 and 88−93 in one monomer and residues of 1−4 and 272−274 in the other monomer are all stabilized by crystal packing. For convenience, we will discuss the subunit architecture in terms of the latter monomer. The NHR is comprised of the N-terminal RNA binding domain (NTD, residues 1−106) and C-terminal catalytic domain (CTD, residues 107−274) (Figure 2A). In the N-terminal domain, four β-strands form a β-sheet, which is surrounded by four α-helices with two on each side. In the C-terminal domain, six β-strands form a parallel β-sheet, which is stabilized by α5, α8, and α10 on one side and α6, α7, α9, and α11 on the other side (Figure 2A). The NTD and CTD interact with each other through inner molecular interactions between α3 and β1 of NTD and α7 and a loop connecting α7 and β7 of CTD. The homodimer is stabilized by extensive intermolecular interactions between α6, α11, and a loop connecting α10 and α11 from each monomeric NHR (Figure 2A).

A characteristic feature of SPOUT MTases is a deep topological knot that binds SAM. This knot is formed by three loops: one is between β8 and β9, one is between β10 and α9, and the other is between β11 and α10. Each monomeric NHR binds to one SAM molecule with the active methyl group of SAM facing toward the N-terminal RNA binding domain of the other NHR molecule in the dimer (Figures 3A and 4A).

Three conserved motifs of SPOUT MTases were found in the CTD of NHR from structure-based sequence alignments (Figure 2B), motif I (G-N-X-G-X3-R), motif II (V/L/I-X2-G-X-E-X2-G), and motif III (I-P-M-X5-S-L-N). Motif III located in the deep knot is the binding site for SAM. Among the motif III, residues Ile, Pro, Met, Ser, Leu, and Asp are highly conserved and involved not only in SAM binding but also in the formation of the dimer interface (Figure 2B).

SAM Binding Site of NHR. In the structure of the NHR complexed with SAM, the overall structure did not undergo

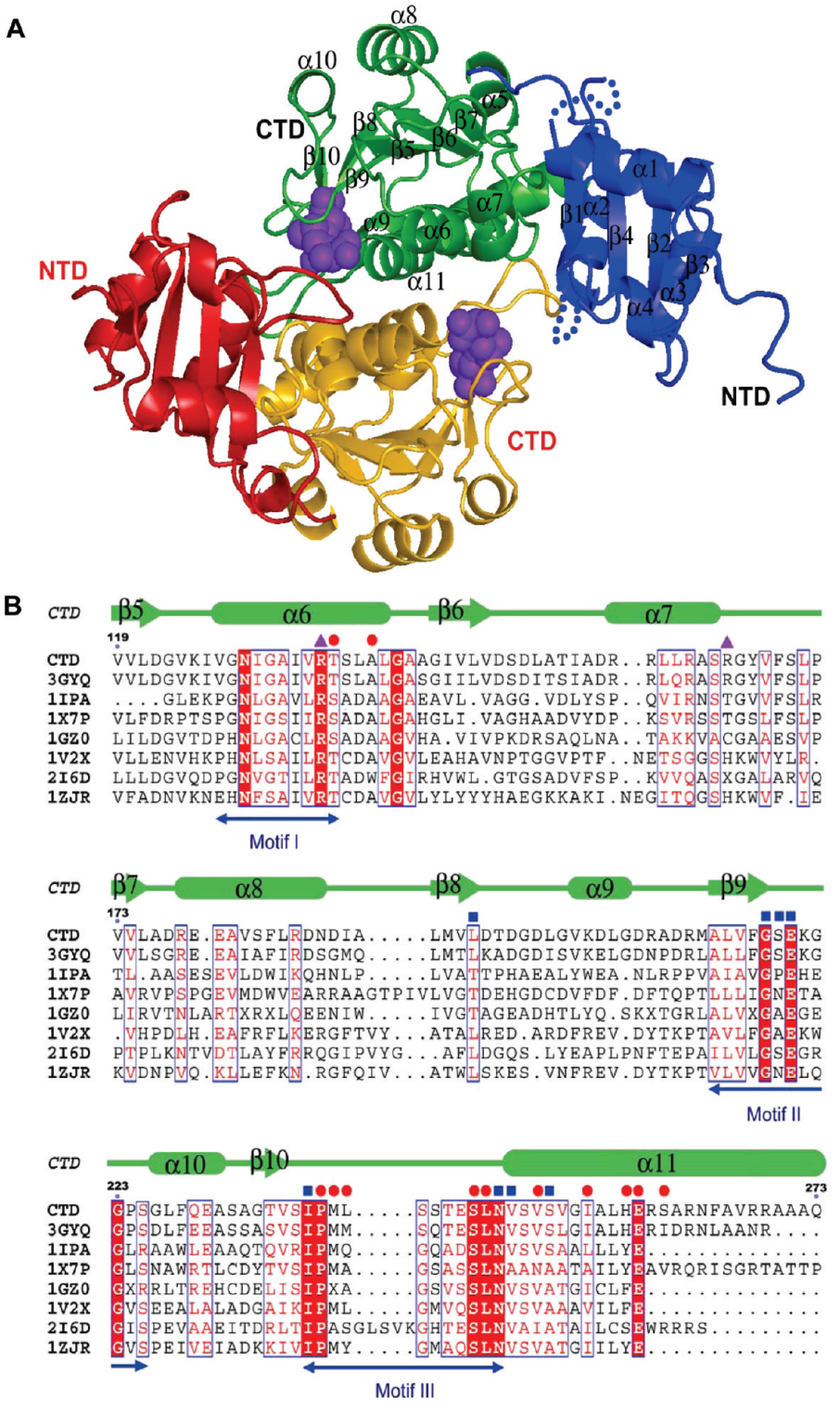

FIGURE 2: Overall structure of the NHR dimer and sequence alignment. (A) Overall structure of the NHR dimer complexed with SAM. Cartoon representation of the NHR structure is colored in blue, green, brown, and red by domains. SAM is shown as a purple sphere. Secondary structural elements are labeled in one NHR monomer. (B) Structure-based sequence alignments. The sequences are named from their PDB accession codes: CTD of NSR protein; 3GYQ, TSR protein from *Streptomyces azureus*; 1IPA, RNA 2′-*O*-ribose methyltransferase from *Thermus thermophilus*; 1X7P, Avirb from *Streptomyces viridochromogenes*; 1GZ0, Rlmb 23S rRNA methyltransferase from *Escherichia coli*; 1V2X, TrmH from *T. thermophilus*; 2I6D, putative RNA methyltransferase of the Trmh family from *Porphyromonas gingivalis*; 1ZJR, class II TrmH tRNA-modifying enzyme from *Aquifex aeolicus*. Identical residues are highlighted with red background, and highly conserved residues are colored in red. Secondary structural elements are colored as in panel A and indicated above the sequences. Residues involved in interaction for the dimer interface, SAM binding of one monomer, and another monomer are indicated by red dots, blue squares, and purple triangles, respectively.

conformational changes upon SAM binding with a rmsd of 0.304 Å for 426 C_α atoms compared to the apo form structure.

In the crystal structure of NHR complexed with SAM, SAM adopts an extended conformation and is stabilized by the topological knot, which is formed by three loops in the C-terminal domain (Figure 3A). Extensive hydrogen bonds are involved in SAM binding to the NHR (Figure 3A,B). In particular, the methionine, methyl group donor, is stabilized by a hydrogen

Table 1: Refinement Statistics of Structures of NHR and NHR in Complex with SAM

protein	NHR	NHR with SAM
resolution (Å)[a]	50.0−2.00 (2.07−2.00)	50.0−2.10 (2.18−2.10)
R_{work}/R_{free} (%)[b]	20.13/25.37	19.57/25.46
deviation from identity		
bonds (Å)	0.008	0.013
angles (deg)	1.216	1.501
average *B* factor (Å^2)	37.51	53.71
Ramachandran plot statistics		
most favored regions (%)	93.7	88.9
allowed regions (%)	4.5	8.2
generously allowed regions (%)	1.3	2.4
disallowed regions (%)	0.4S	0.4

[a]The values for the data in the highest resolution shell are shown in parentheses. [b]$R_{free} = \sum_{Test}||F_o| - |F_c||/\sum_{Test}|F_o|$, where Test is a test set of about 5% of the total reflections randomly chosen and set aside prior to refinement for the complex.

bond between the positive charge on the sulfur and Ser 219, with the methyl donor group facing outward. The N-terminal methionine tail of SAM is checked with five hydrogen bonds, through interactions with Val249, Asn248, Arg135, and Arg165 from the other NHR molecule in the dimer. The adenosine ring is stabilized by three hydrogen bonds between the backbone oxygen of Ile238 and amino groups A-N6 and A-N1 as well as the γ oxygen of Ser-252 and A-N9. Hydrophobic interactions between SAM and Ser237, Asp196, Ser246, Leu247, and Glu220 also contribute to positioning the SAM molecule. All residues involved in SAM binding are highly conserved, indicating their critical role for the function (Figure 2B).

To further study the contribution of SAM binding for NHR activity, we measured the *in vitro* methyltransferase activity assay of various NHR mutants. The results showed that mutation of S219A slightly decreased the activity, mutation of E220Q only had about 10% activity, and mutation of R135A, R165A abolished or significantly decreased (about 5%) the activity for both 60 base and 29 base RNA substrates (Figure 3D). The minimal effect of mutation of S219A suggests that stabilization of sulfur may not be very important for methyltransferase activity. It can be explained that both sides of the sulfur have been fixed through extensive interactions between SAM and NHR, and the relative flexibility of the active methyl group has no effect on methyltransferase activity. However, the stabilization of the N-terminus of SAM is very important because mutations of E220Q, R135A, and R165A significantly decreased or abolished methyltransferase activity (Figure 3D). The results are also consistent with structural data showing weak electron density for atoms between sulfur and the N-terminus with flexible conformation and better electron density for the adenosine ring with fixed conformation (Figure 3C).

We speculate the methylation of the 2′-O of A1067 could be further promoted by the ability of an adjacent base to pick up the dissociating proton. Such a candidate base would be positioned on the other side of the 2′-OH of the substrate RNA relative to the SAM to receive the proton as part of the S_N2 reaction. The only available base close to the sulfur of SAM that could accommodate the insertion of the substrate RNA for methyl group transfer is Arg135 in the neighboring NHR of the dimer (Figure 3A). In addition, we also noticed that mutation of R135A abolished the activity, suggesting that the residue may indeed provide a proton acceptor for the 2′-OH of A1067 during the methylation of 23S rRNA.

Dimer Interface of NHR. The homodimer is stabilized by extensive intermolecular interactions between two NHR molecules (Figures 2A and 4A). The dimerization is mainly mediated by the interaction between α6, α11, and a loop connecting α10 and α11 from each monomeric NHR molecule. Many residues are involved in the dimer interface with a buried surface area of 1304.7 Å^2 for one subunit. In particular, the hydrophobic interactions between α11 and α11′ involve the side chains of M240, L247, V251, I255, and F265 from both monomers. An important hydrogen bond between E259 of α11 and H258 of α11′ contributes to the binding interface. P239 of α11 and S261′ and H258′ of α11′ form hydrogen bonds mediated by a water molecule, W73. Residues of N248, S246, and L241 of α11 interact with residues of T136, R135, and A139 of α6′, respectively, through forming hydrogen bonds (Figure 4A).

To investigate the importance of the dimer interface, sequence conservation was projected onto the surface of monomeric NHR and colored according to the conservation scores which were calculated using the ConSurf Server (*44*) (http://consurf.tan.ac.il) (Figure 4B). The striking pattern of colored surface indicated that the residues on the dimer interface are invariant or highly conserved, which also supports the importance of dimerization of NHR from an evolutionary point of view.

Structural analysis showed that residues H258 and E259 are involved in the formation of the dimer interface and both residues are highly conserved (Figure 2B). The double mutation of H258A, E259A decreased the methyltransferase activity to 40% compared to that of the wild-type protein, indicating that residues involved in dimer formation did affect the enzymatic activity to some extent (Figure 3D). We also made mutations of more residues involved in dimer formation to test the requirement for enzymatic activity. However, the mutants were not soluble in the *E. coli* expression system, and the corresponding activities were not measured. The structural analysis and enzymatic activity data suggest that dimerization is required for NHR-mediated methylation of 23S rRNA substrate.

Enzymatic Activity of the N-Terminal RNA Binding Domain of NHR. Extensive efforts were made to obtain the structure of the NHR−RNA complex without success. To study the interaction between the N-terminal RNA binding domain and 23S rRNA, we performed a Dali search (*43*) of the NHR N-terminal domain versus all known structures in the Protein Data Bank. Among 514 entries with structural similarity (*Z* score higher than 2.0), the top three protein RNA complex structures with a *Z* score higher than 8.0 were selected for the following structural comparison. The three structures are the yeast ribosomal protein L30e complex with the internal loop of pre-mRNA (1T0K.pdb) (*45*), spliceosomal 15.5 kDa protein bound to U4 snRNA (2OZB.pdb) (*46*), and the L7Ae protein complex with rRNA (1SDS.pdb) (*47*). Structural comparison showed that NHR and the three proteins adopt a similar α/β/α sandwich fold and superimpose well (Figure 5A). The three RNA molecules also superimpose well, especially in the protein binding region. Three loops involved in RNA binding in the three protein RNA complexes are compared (Figure 5A−D). Here, we designated the three loops L1, L2, and L3 for convenience. In the NHR structure, the corresponding loops, L1 (residues 35−37), L2 (residues 57−64), and L3 (residues 89−96), are predicted to be important for RNA recognition and the methyltransferase activity (Figure 5E). Sequence alignment showed that L1, L2, and L3 are not conserved, indicating that these loops may determine the substrate specificity (Figure 5G). By structural

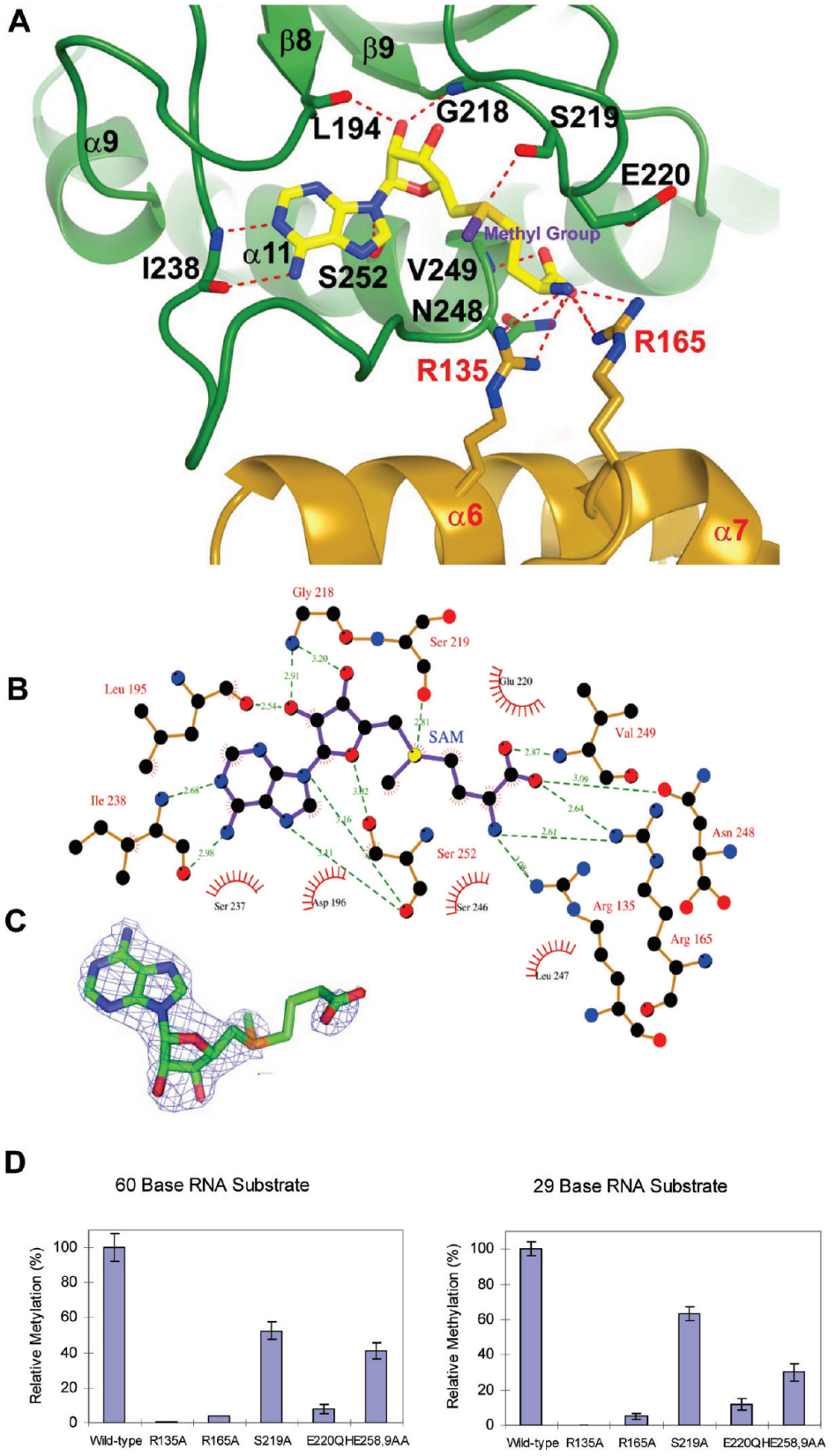

FIGURE 3: SAM binding site of NHR. (A) Structure of SAM binding site. Detailed interactions between SAM and NHR are shown. SAM and side chains in NHR involved in interaction are shown in stick representation and colored as in Figure 2B. The active methyl group of SAM is colored in purple. Secondary structural elements and residue numbers for two monomers are labeled in black and red, respectively. Hydrogen bonds are represented by magenta dotted lines. (B) Ligplot representation of the interactions between SAM and NHR. The carbon, oxygen, and nitrogen are colored in black, red, and blue, respectively. Lengths of hydrogen bonds (dashed lines) are given in angstroms. Hydrophobic interactions are also indicated. (C) Electron density ($2F_o - F_c$) map covering SAM at a resolution of 2.1 Å is shown. The map is contoured at 1.0σ, and SAM is shown in stick representation. (D) Methyltransferase activity of wild type and mutations of residues involved in SAM binding and dimer formation.

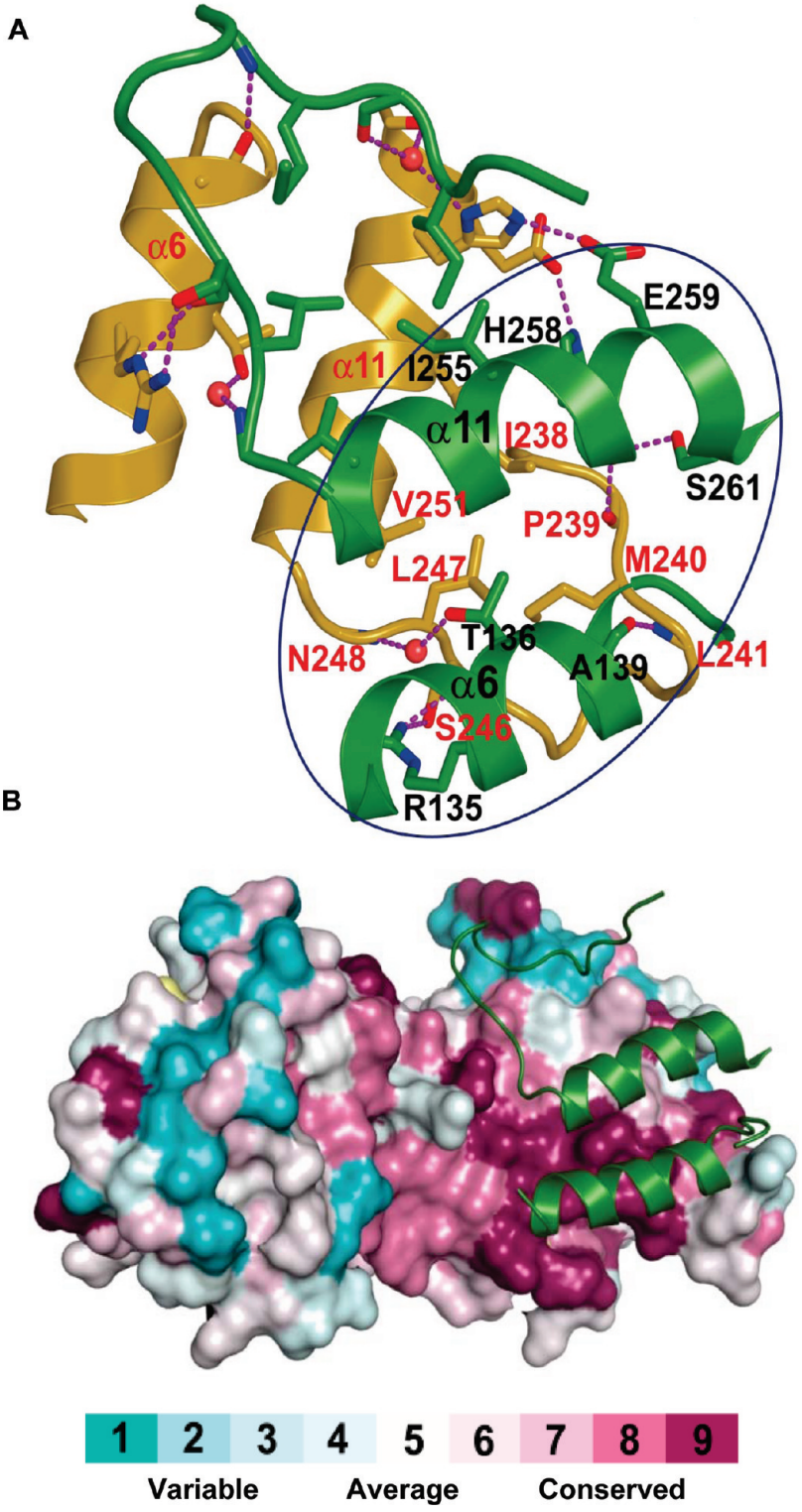

FIGURE 4: Dimer interface of NHR. (A) Structure of the NHR dimer interface. Detailed interactions between two NHR monomers are shown, and symmetric dimer interface is circled. Side chains involved in dimerization are shown in stick representation and colored as in Figure 2B. Secondary structural elements and residue numbers for two monomers are labeled in black and red, respectively. Hydrogen bonds are represented by magenta dotted lines, and water is represented by a red ball. (B) Sequence conservation projected on the surface of one NHR monomer, which is shown in surface model and colored according to the conservation scores. The secondary structure involved in dimer formation in the other NHR monomer is shown as a cartoon representation and colored in green. Color codes are indicated.

comparison, we docked the RNA structure into the N-terminal domain of NHR, showing a similar binding mode as in the L30−RNA complex structure (Figure 5F).

To confirm our analyses and structure model, we performed the *in vitro* methyltransferase activity assay using NHR mutants to study the importance of the three loops. The results showed that mutation of E35A, D36A in L1 abolished or significantly decreased the enzymatic activity, indicating that the small loop L1 is important for methyltransferase activity and RNA recognition (Figure 5H). Mutations of E91A and R92A significantly decreased or abolished the enzymatic activity, respectively, indicating that L3 also plays critical role in the methyltransferase

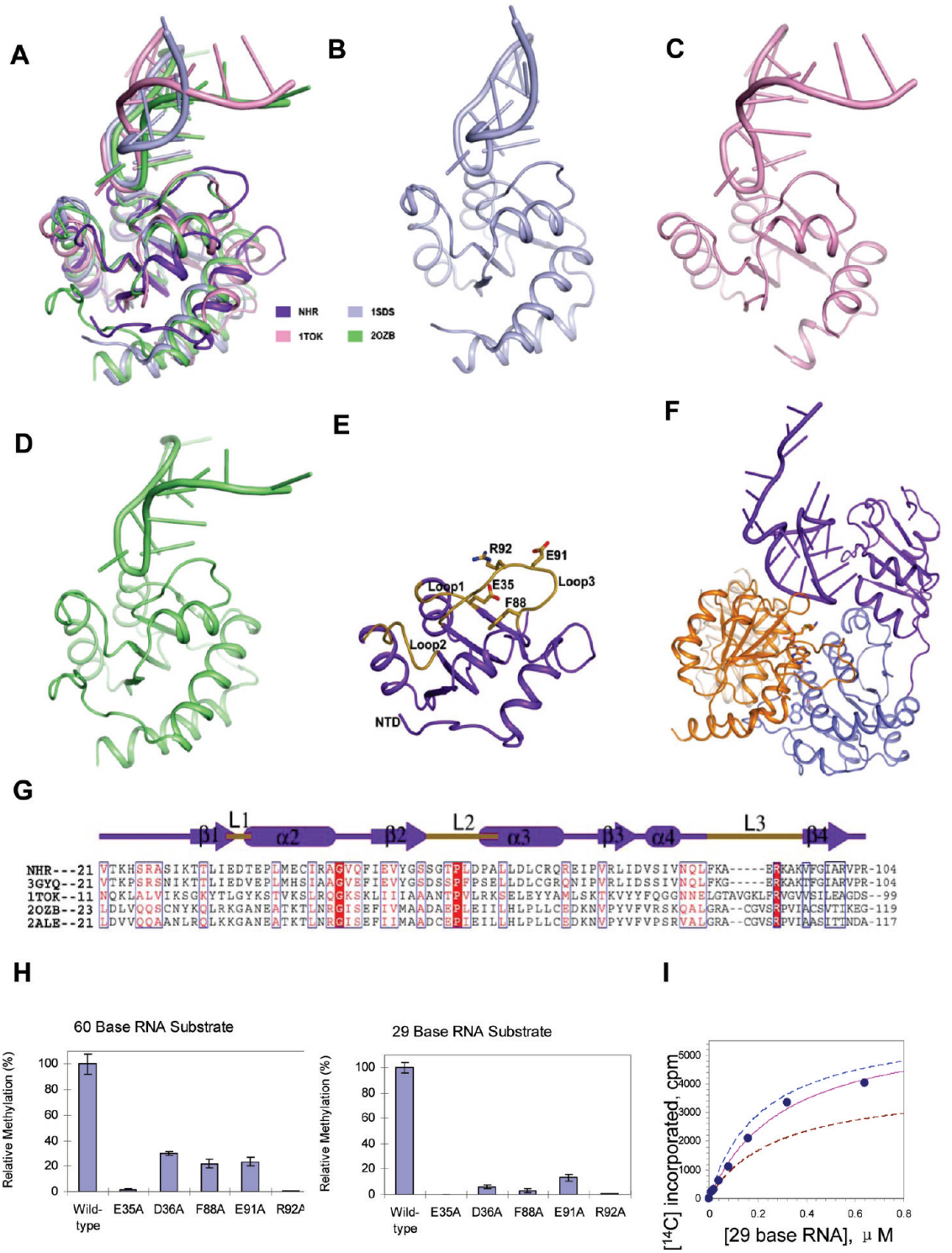

FIGURE 5: Structure comparison and structure model of NTD of NHR. (A) Structure comparison of NTD of NHR with L30, spliceosomal 15.5 kDa protein, and L7Ae complexed with RNA. Color codes are indicated. (B) Structure of the L30 complex with RNA, shown in blue. (C) Structure of spliceosomal 15.5 kDa protein complex with RNA, shown in pink. (D) Structure of the L7Ae complex with RNA, shown in green. (E) Structure of the N-terminal domain of NHR, shown in purple. Speculated residues for RNA recognition are shown in yellow. L1, L2, and L3 loops are labeled. (F) Structure model for NHR in complex with its substrate *E. coli* 29 base 23S rRNA. (G) Structure-based sequence alignment of the N-terminal domain of NHR, TSR, and three above-mentioned proteins, with their PDB numbers. (H) Methyltransferase activity of wild type and mutations of residues in loops L1 and L3. (I) Methyltransferase activity of the NHR mutant of the swapped L2 loop (with the L2 loop replaced by the corresponding residues of TSR) with the 29 base RNA as substrate, shown as a purple line. The controls for NHR and TSR are indicated as blue and brown dashed lines, respectively.

mechanism (Figure 5H). Mutation of F88A also significantly decreased the activity, which is consistent with the results from mutation of F88A on TSR (Figure 5H) (*15*). However, unlike the corresponding residue in L30 with the side chain of F85 facing outside for RNA binding, F88 in both NHR and TSR are facing inside to the N-terminal domain and mainly involved in hydrophobic core formation. The decreased activity may result in the possibly increased flexibility of the L3 loop without the stabilization

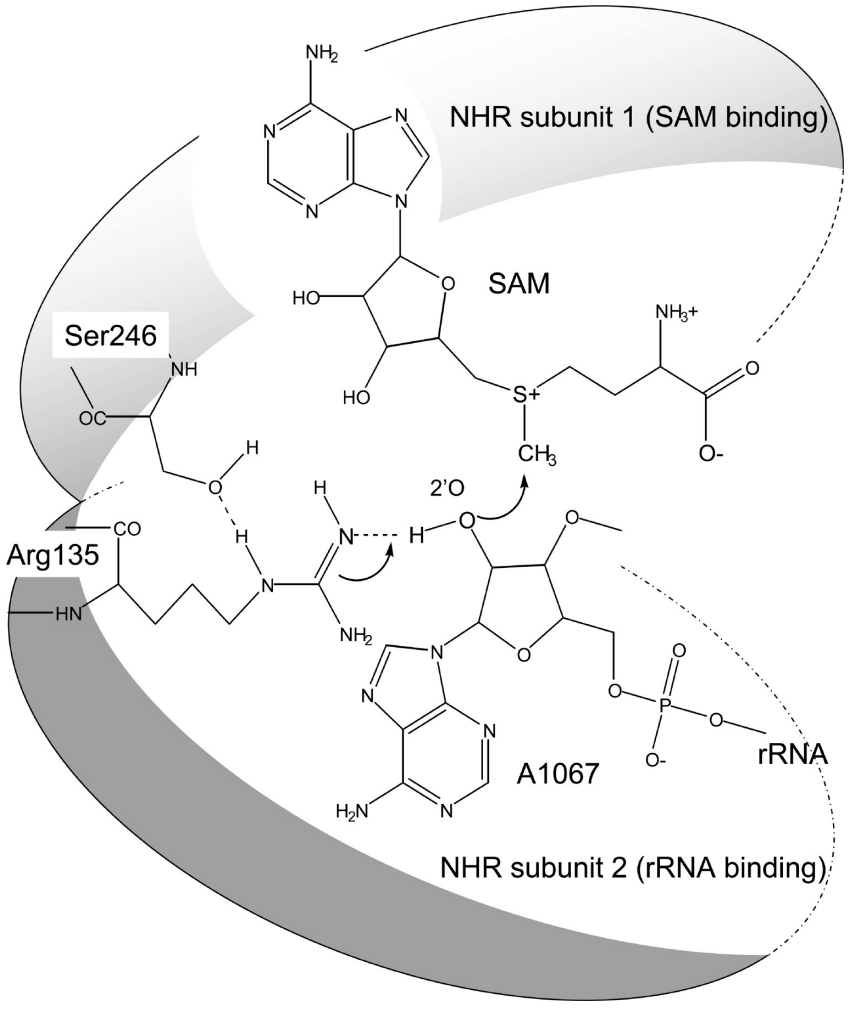

FIGURE 6: Proposed scheme for transfer of the methyl group by NHR. The methyl group donor, SAM, is bound to one subunit of the homodimer, and the 2′-hydroxyl of the substrate nucleotide A1067 is positioned adjacent to the methyl group in the active site of the enzyme, between the two subunits. The transfer of the methyl group is probably catalyzed by Arg135 from the second subunit, which withdraws a proton from the 2′-hydroxyl of A1067 during methylation.

of F88 (Figure 5H). We compared the sequence of THR and NSR and found that the residues within L2 are different to each other, although THR and NSR have 74% similarity in sequence. To study whether L2 is important for activity, we made an NHR mutation with L2 (residues 57−64) replaced by the corresponding residues from TSR and measured the methyltransferase activity, which showed that the NHR mutant has similar enzymatic activity to the NHR protein (Figure 5I). Mutants in which all residues of L2 were changed to alanine were not soluble in expression, and the corresponding enzymatic activities were not measured. The results indicate that L2 only plays a minor role for NHR methyltransferase activity.

DISCUSSION

RNA Recognition. In this report, we determined the crystal structure of NHR and NHR in complex with SAM. Comprehensive structural and biochemical analyses demonstrated that loops in CTD for SAM binding and loops L1 and L3 in NTD are important for methyltransferase activity *in vitro* with 29 nucleotide and 60 nucleotide RNA as substrates. Initial attempts to measure binding affinities between NHR mutants and substrate RNA molecules by fluorescence anisotropy measurements were compromised by the precipitation of a number of mutant proteins at higher concentrations; for this reason we considered methylation activity to be a more accurate readout of methyltransferase function. Hence, we present methyltransferase activity for wild-type and mutant proteins of NHR. The structural and biochemical analyses, including structural comparison to other protein RNA complexes, are consistent with each other, which allow us to discuss the RNA recognition represented by the enzymatic results on the N-terminal domain.

The natural substrate for NHR and TSR is 23S rRNA. Both enzymes specifically transfer a methyl group to the 2′-hydroxyl of base A1067, which overlaps with the site in the ribosome and where the two antibiotics (thiostrepton and nosiheptide) bind. Both NHR and TSR can bind and methylate the model RNA substrates: the 29 nucleotide and the 60 nucleotide RNA construct. Base A1067 is positioned in a region of rRNA that folds to adopt a specific tertiary structure. It is therefore informative to note that the shorter 29 nucleotide RNA was a more efficient substrate for both enzymes (Figure 1C−F). It is also a reasonable speculation that the 29 nucleotide RNA adopts a conformation more similar to that of the natural substrate, which has better accessibility to NHR/TSR than that of 60 base RNA. Because the methylation occurs before assembly of the ribosome (*48*), it remains unknown what conformation the natural substrate adopts *in vivo*, which will provide evidence to reveal the mechanism of the methylation on A1067 of 23S rRNA.

Mechanism of Catalysis. NHR shares a common fold with the SpoU (TrmH) tRNA methyltransferases for which a catalytic mechanism has been proposed (*34*). SpoU is a 2′-OH methyltransferase that methylates G18 in tRNA. Comparison of the two crystal structures combined with our mutational analysis allows us to propose a catalytic mechanism for NHR that closely resembles that of other members of the SpoU family. Like SpoU, NHR forms an active dimer in solution, which is also consistent with the SpoU catalytic model in which one subunit binds SAM and the second subunit also binds SAM. In the SpoU catalytic model, intersubunit hydrogen bonding between the conserved residues Arg41 and Ser150 defines the catalytic center and orients Arg41 so that it abstracts the 2′-hydroxyl proton to allow nucleophilic attack by the 2′-oxygen of G18 on the methyl group of SAM. On the basis of the structural and biochemical studies in this work, we propose that Arg135 is oriented by intersubunit hydrogen bonding to Ser246, such that Arg135 would act as the base that abstracts the 2′-hydroxyl proton to allow nucleophilic attack by the 2′-oxygen of A1067 on the methyl group of SAM as detailed in Figure 6. A similar working model was also found in TrmD, in which Arg154 acts as the proton acceptor.

Comparison between NHR and TSR Structures. When this report was in preparation, Dunstan et al. reported the crystal structure of the TSR complex with SAM (*15*). Structures of NHR and TSR are superimposed well with a rmsd of 3.068 Å for 459 C_α atoms (for overall structure), 0.693 Å for 80 C_α atoms (for NTD), and 0.544 Å for 143 C_α atoms (for CTD) if compared with individual domains. This is not surprising because the two proteins share 74% sequence identity and target the same substrate (Supporting Information Figure S1). Thus, the structural information revealed by the two structures is similar. However, there are three major differences between these two independent studies. First, comprehensive structural analysis and methyltransferase activity assays of NHR identified critical regions for SAM binding in CTD and RNA binding in NTD, including critical residues for these functions. These systematic studies revealed that substrate recognition by NHR is determined by loops L1 and L3, which were not addressed in TSR paper (*15*). The different activities between NHR and TSR for the 29 base RNA were quantified, and the underlying mechanism of recognition was further revealed based on structural and biochemical analyses allowing us to conclude that L2 plays a minor role in the differential activities of the two proteins. Second, we found that mutation of R135A abolished the enzymatic activity and proposed that this residue is the proton acceptor for the methylation of substrate RNA. Finally, we note that the side chains of F88 in NHR and TSR face inside and are stabilized in the hydrophobic core of the NTD, and our NHR−RNA modeling suggests that they are unlikely to invert to interact with RNA; the detailed interactions between NHR/TSR and RNA are not necessarily similar to those of the L30−RNA complex.

Although we have shown that dimerization is required for NHR activity, and probably plays an important role in the selection and enzymatic methylation of the substrate nucleotide, we cannot discern whether the recognition of the substrate RNA molecule overall by NHR occurs in the same or different subunit molecules within the dimer. We anticipate that an NHR−RNA cocrystal structure will reveal further details of the way this protein recognizes its RNA substrate and the specific mechanism of methyl group transfer.

ACKNOWLEDGMENT

We thank all staff members of beamline BL17U at SSRF (China) and BL17A at Photon Factory (Japan) for help with data collection.

SUPPORTING INFORMATION AVAILABLE

Figure S1, sequence alignment of NHR and TSR (the homology between the NHR and TSR is 74%); Figure S2, overall structure of the apo form of the NHR dimer (cartoon representation of the NHR structure is colored in blue, green, brown, and red by domains; secondary structural elements are labeled in one NHR monomer). This material is available free of charge via the Internet at http://pubs.acs.org.

REFERENCES

1. Wimberly, B. T., Brodersen, D. E., Clemons, W. M., Jr., Morgan-Warren, R. J., Carter, A. P., Vonrhein, C., Hartsch, T., and Ramakrishnan, V. (2000) Structure of the 30S ribosomal subunit. *Nature 407*, 327–339.
2. Ban, N., Nissen, P., Hansen, J., Moore, P. B., and Steitz, T. A. (2000) The complete atomic structure of the large ribosomal subunit at 2.4 Å resolution. *Science 289*, 905–920.
3. Harms, J., Schluenzen, F., Zarivach, R., Bashan, A., Gat, S., Agmon, I., Bartels, H., Franceschi, F., and Yonath, A. (2001) High resolution structure of the large ribosomal subunit from a mesophilic eubacterium. *Cell 107*, 679–688.
4. Yusupov, M. M., Yusupova, G. Z., Baucom, A., Lieberman, K., Earnest, T. N., Cate, J. H., and Noller, H. F. (2001) Crystal structure of the ribosome at 5.5 Å resolution. *Science 292*, 883–896.
5. Knowles, D. J., Foloppe, N., Matassova, N. B., and Murchie, A. I. (2002) The bacterial ribosome, a promising focus for structure-based drug design. *Curr. Opin. Pharmacol. 2*, 501–506.
6. Ramakrishnan, V. (2002) Ribosome structure and the mechanism of translation. *Cell 108*, 557–572.
7. Farrow, K. A., Lyras, D., and Rood, J. I. (2000) The macrolide-lincosamide-streptogramin B resistance determinant from *Clostridium difficile* 630 contains two erm(B) genes. *Antimicrob. Agents Chemother. 44*, 411–413.
8. Kovalic, D., Giannattasio, R. B., Jin, H. J., and Weisblum, B. (1994) 23S rRNA domain V, a fragment that can be specifically methylated in vitro by the ErmSF (TlrA) methyltransferase. *J. Bacteriol. 176*, 6992–6998.
9. Vester, B., and Douthwaite, S. (1994) Domain V of 23S rRNA contains all the structural elements necessary for recognition by the ErmE methyltransferase. *J. Bacteriol. 176*, 6999–7004.
10. Ohta, T., and Hasegawa, M. (1993) Analysis of the self-defense gene (fmrO) of a fortimicin A (astromicin) producer, *Micromonospora olivasterospora*: comparison with other aminoglycoside-resistance-encoding genes. *Gene 127*, 63–69.
11. Mosbacher, T. G., Bechthold, A., and Schulz, G. E. (2005) Structure and function of the antibiotic resistance-mediating methyltransferase AviRb from *Streptomyces viridochromogenes*. *J. Mol. Biol. 345*, 535–545.
12. Michel, G., Sauve, V., Larocque, R., Li, Y., Matte, A., and Cygler, M. (2002) The structure of the RlmB 23S rRNA methyltransferase reveals a new methyltransferase fold with a unique knot. *Structure 10*, 1303–1315.
13. Lentzen, G., Klinck, R., Matassova, N., Aboul-ela, F., and Murchie, A. I. (2003) Structural basis for contrasting activities of ribosome binding thiazole antibiotics. *Chem. Biol. 10*, 769–778.
14. Bechthold, A., and Floss, H. G. (1994) Overexpression of the thiostrepton-resistance gene from *Streptomyces azureus* in *Escherichia coli* and characterization of recognition sites of the 23S rRNA A1067 2′-methyltransferase in the guanosine triphosphatase center of 23S ribosomal RNA. *Eur. J. Biochem. 224*, 431–437.
15. Dunstan, M. S., Hang, P. C., Zelinskaya, N. V., Honek, J. F., and Conn, G. L. (2009) Structure of the thiostrepton resistance methyltransferase·*S*-adenosyl-L-methionine complex and its interaction with ribosomal RNA. *J. Biol. Chem. 284*, 17013–17020.
16. Thompson, J., Schmidt, F., and Cundliffe, E. (1982) Site of action of a ribosomal RNA methylase conferring resistance to thiostrepton. *J. Biol. Chem. 257*, 7915–7917.
17. Dosch, D. C., Strohl, W. R., and Floss, H. G. (1988) Molecular cloning of the nosiheptide resistance gene from *Streptomyces actuosus* ATCC 25421. *Biochem. Biophys. Res. Commun. 156*, 517–523.

18. Li, Y., Dosch, D. C., Strohl, W. R., and Floss, H. G. (1990) Nucleotide sequence and transcriptional analysis of the nosiheptide-resistance gene from *Streptomyces actuosus*. *Gene 91*, 9–17.
19. Prange, T., Ducruix, A., Pascard, C., and Lunel, J. (1977) Structure of nosipeptide, a polythiazole-containing antibiotic. *Nature 265*, 189–190.
20. Endo, T., and Yonehara, H. (1978) Identity of multhiomycin with nosiheptide. *J. Antibiot.* (*Tokyo*) *31*, 623–625.
21. Cromwell, G. L., Stahly, T. S., Speer, V. C., and O'Kelly, R. (1984) Efficacy of nosiheptide as a growth promotant for growing-finishing swine—a cooperative study. *J. Anim. Sci. 59*, 1125–1128.
22. Rodnina, M. V., Savelsbergh, A., Matassova, N. B., Katunin, V. I., Semenkov, Y. P., and Wintermeyer, W. (1999) Thiostrepton inhibits the turnover but not the GTPase of elongation factor G on the ribosome. *Proc. Natl. Acad. Sci. U.S.A. 96*, 9586–9590.
23. Cameron, D. M., Thompson, J., March, P. E., and Dahlberg, A. E. (2002) Initiation factor IF2, thiostrepton and micrococcin prevent the binding of elongation factor G to the *Escherichia coli* ribosome. *J. Mol. Biol. 319*, 27–35.
24. Wimberly, B. T., Guymon, R., McCutcheon, J. P., White, S. W., and Ramakrishnan, V. (1999) A detailed view of a ribosomal active site: the structure of the L11-RNA complex. *Cell 97*, 491–502.
25. Harms, J. M., Wilson, D. N., Schluenzen, F., Connell, S. R., Stachelhaus, T., Zaborowska, Z., Spahn, C. M., and Fucini, P. (2008) Translational regulation via L11: molecular switches on the ribosome turned on and off by thiostrepton and micrococcin. *Mol. Cell 30*, 26–38.
26. Bower, J., Drysdale, M., Hebdon, R., Jordan, A., Lentzen, G., Matassova, N., Murchie, A., Powles, J., and Roughley, S. (2003) Structure-based design of agents targeting the bacterial ribosome. *Bioorg. Med. Chem. Lett. 13*, 2455–2458.
27. Egebjerg, J., Douthwaite, S. R., Liljas, A., and Garrett, R. A. (1990) Characterization of the binding sites of protein L11 and the L10·(L12)4 pentameric complex in the GTPase domain of 23 S ribosomal RNA from *Escherichia coli*. *J. Mol. Biol. 213*, 275–288.
28. Jonker, H. R., Ilin, S., Grimm, S. K., Wohnert, J., and Schwalbe, H. (2007) L11 domain rearrangement upon binding to RNA and thiostrepton studied by NMR spectroscopy. *Nucleic Acids Res. 35*, 441–454.
29. Schmidt, F. J., Thompson, J., Lee, K., Dijk, J., and Cundliffe, E. (1981) The binding site for ribosomal protein L11 within 23 S ribosomal RNA of *Escherichia coli*. *J. Biol. Chem. 256*, 12301–12305.
30. Conn, G. L., Draper, D. E., Lattman, E. E., and Gittis, A. G. (1999) Crystal structure of a conserved ribosomal protein-RNA complex. *Science 284*, 1171–1174.
31. Gutell, R. R., Larsen, N., and Woese, C. R. (1994) Lessons from an evolving rRNA: 16S and 23S rRNA structures from a comparative perspective. *Microbiol. Rev. 58*, 10–26.
32. Robinow, C., and Kellenberger, E. (1994) The bacterial nucleoid revisited. *Microbiol. Rev. 58*, 211–232.
33. Gustafsson, C., Reid, R., Greene, P. J., and Santi, D. V. (1996) Identification of new RNA modifying enzymes by iterative genome search using known modifying enzymes as probes. *Nucleic Acids Res. 24*, 3756–3762.
34. Watanabe, K., Nureki, O., Fukai, S., Endo, Y., and Hori, H. (2006) Functional categorization of the conserved basic amino acid residues in TrmH (tRNA (Gm18) methyltransferase) enzymes. *J. Biol. Chem. 281*, 34630–34639.
35. Liu, J., Wang, W., Shin, D. H., Yokota, H., Kim, R., and Kim, S. H. (2003) Crystal structure of tRNA (m1G37) methyltransferase from *Aquifex aeolicus* at 2.6 Å resolution: a novel methyltransferase fold. *Proteins 53*, 326–328.
36. Elkins, P. A., Watts, J. M., Zalacain, M., van Thiel, A., Vitazka, P. R., Redlak, M., Andraos-Selim, C., Rastinejad, F., and Holmes, W. M. (2003) Insights into catalysis by a knotted TrmD tRNA methyltransferase. *J. Mol. Biol. 333*, 931–949.
37. Watanabe, K., Nureki, O., Fukai, S., Ishii, R., Okamoto, H., Yokoyama, S., Endo, Y., and Hori, H. (2005) Roles of conserved amino acid sequence motifs in the SpoU (TrmH) RNA methyltransferase family. *J. Biol. Chem. 280*, 10368–10377.
38. Yang, H., Wang, P., Dong, Z., Li, X., Gong, R., Yang, Y., Li, Z., Xu, Y., and Xu, Y. (2010) Crystallization and preliminary crystallographic analysis of nosiheptide-resistance methyltransferase from *Streptomyces actuosus* in complex with SAM. *Acta Crystallogr. 66*, 579–582.
39. Otwinowski, Z., and Minor, W. (1997) Processing of X-ray diffraction data collected in oscillation mode. *Methods Enzymol. 276*, 307–326.
40. Adams, P. D., Grosse-Kunstleve, R. W., Hung, L. W., Ioerger, T. R., McCoy, A. J., Moriarty, N. W., Read, R. J., Sacchettini, J. C., Sauter, N. K., and Terwilliger, T. C. (2002) PHENIX: building new software for automated crystallographic structure determination. *Acta Crystallogr., Sect. D: Biol. Crystallogr. 58*, 1948–1954.
41. Emsley, P., and Cowtan, K. (2004) Coot: model-building tools for molecular graphics. *Acta Crystallogr., Sect. D: Biol. Crystallogr. 60*, 2126–2132.
42. Laskowski, R. A., MacArthur, M. W., Moss, D. S., and Thornton, J. M. (1993) PROCHECK: a program to check the stereochemical quality of protein structures. *J. Appl. Crystallogr. 26*, 283–291.
43. Holm, L., Kaariainen, S., Rosenstrom, P., and Schenkel, A. (2008) Searching protein structure databases with DaliLite v.3. *Bioinformatics 24*, 2780–2781.
44. Landau, M., Mayrose, I., Rosenberg, Y., Glaser, F., Martz, E., Pupko, T., and Ben-Tal, N. (2005) ConSurf 2005: the projection of evolutionary conservation scores of residues on protein structures. *Nucleic Acids Res. 33*, W299–W302.
45. Chao, J. A., and Williamson, J. R. (2004) Joint X-ray and NMR refinement of the yeast L30e-mRNA complex. *Structure 12*, 1165–1176.
46. Liu, S., Li, P., Dybkov, O., Nottrott, S., Hartmuth, K., Luhrmann, R., Carlomagno, T., and Wahl, M. C. (2007) Binding of the human Prp31 Nop domain to a composite RNA-protein platform in U4 snRNP. *Science* (*New York*) *316*, 115–120.
47. Hamma, T., and Ferre-D'Amare, A. R. (2004) Structure of protein L7Ae bound to a K-turn derived from an archaeal box H/ACA sRNA at 1.8 Å resolution. *Structure 12*, 893–903.
48. Cundliffe, E., and Thompson, J. (1979) Ribose methylation and resistance to thiostrepton. *Nature 278*, 859–861.